Desalination and Water Treatment
www.deswater.com

doi: 10.1080/19443994.2015.1036784

57 (2016) 10730–10744
May

Taylor & Francis
Taylor & Francis Group

Nanocomposite of carbon nanotubes/silica nanoparticles and their use for adsorption of Pb(II): from surface properties to sorption mechanism

Tawfik A. Saleh

Department of Chemistry, King Fahd University of Petroleum & Minerals, Dhahran, Saudi Arabia, Tel. +966 3 860 1734; Fax: +966 3 860 4288; emails: tawfik@kfupm.edu.sa, tawfikas@hotmail.com

Received 23 January 2015; Accepted 28 March 2015

ABSTRACT

This paper demonstrates the synthesis of multi-wall carbon nanotubes and silica nanocomposite (CNT/SiO_2). Successful realization of MWCNT/SiO_2 nanostructure was observed by scanning electron microscopy, energy dispersive X-ray spectroscopy, Fourier transform infrared spectroscopy and high-resolution transmission electron microscopy studies. The as-prepared nanocomposite was evaluated as an adsorbent to remove lead, Pb(II), from aqueous solutions. The resulting MWCNT/SiO_2 manifests propitious adsorption performance (~95%) over silica nanoparticles (~50%) and CNTs (~45%). Lagergren's pseudo-first order, pseudo-second order and intraparticle diffusion models were used to analyse the kinetic data obtained at different initial Pb(II) concentrations. The adsorption kinetic data were described well by the pseudo-second order model with R^2 of 0.99. The activation energy (E_a) of the adsorption process was calculated as 15.8 kJ mol^{-1}. Adsorption data were described well by the Langmuir and Temkin models. The positive values of both ΔH° (29.4 kJ/mol) and ΔS° (116.8 J/mol K) obtained suggest an endothermic reaction and in increase in randomness at the solid–liquid interface during the adsorption of Pb(II) on the nanocomposite. The negative ΔG° values indicate a spontaneous adsorption process. Elemental dispersive X-ray analysis and mapping confirmed the adsorption of Pb(II) on the nanocomposite surface. The work also highlights the recyclability of the nanocomposite with high efficiencies and supports its potential for environmental applications. It is anticipated that the results bear broad potential in the sorption domain for the design of efficient and reusable adsorbent.

Keywords: Carbon nanotubes/silica; Adsorption; Pb(II); Kinetic; Thermodynamic

1. Introduction

Heavy metals are released into the surface and groundwater because of various activities such as electroplating, and pigment and paint manufacturing. Because of their toxicity and tendency to bioaccumulation, the removal of metals from industrial effluents before discharge into the environment is required to mitigate any impact on plants, animals and humans [1]. Lead is one of the most toxic metals that are widely used in various industries, such as battery and glass manufacturing; metal plating and finishing; printing and tanning [2]. The permissible levels of lead in drinking and wastewater are 0.005 and 0.05 mg/L, respectively [3].

Several conventional methods, such as chemical precipitation as hydroxides, carbonates or sulphides and subsequent liquid–solid separation, sorption, membrane processes, reverse osmosis, electrolytic recovery and liquid–liquid extraction, are used for the removal of pollutants [4,5]. However, these technologies are either expensive for the treatment and disposal of the secondary toxic sludge or ineffective when the toxic metal is present in wastewaters at low concentrations [6]. Alternatively, adsorption is one of the preferred methods for the treatment of wastewater because of its efficiency and simplicity. A successful adsorption process depends on the adsorption performance of the adsorbents.

Various conventional adsorbents such as activated carbon have been reported for the removal of metal from wastewaters [6,7]. Other materials, such as clay, metal hydroxides, metal oxides, bentonite and zeolites, have been reported for the removal of metal ions such as lead [4,8,9]. Silica gel, silica nanoparticles, functionalized silica, carbonated tricalcium silicate and silica gel containing sulphur, nitrogen and oxygen as adsorb centres have been reported for heavy metal ions adsorption from aqueous/ethanolic solutions [10–12].

Carbon nanotubes (CNTs) have attracted attention due to their chemical and mechanical stability and large specific surface area [13]. Oxidized CNTs with H_2O_2, $KMnO_4$, and HNO_3 have been reported to show adsorption capability, and high adsorption efficiency for sorption of heavy metals such as lead, cadmium and uranium [14]. Oxidized CNTs show enhanced adsorption capacities due to the functional groups introduced by oxidation compared with the as-grown CNTs [15].

The application of nanomaterials for the adsorption of pollutants has arisen as an interesting area of research due to their higher surface area and greater active sites for interaction with pollutants. However, the agglomeration of the nanoparticles is considered as a major drawback. Composite fabrication is expected to reduce their agglomeration. CNTs bonded fused-silica fibre has been reported for solid phase micro extraction with gas chromatographic analysis of phenols in contaminated water [16]. CNT reinforced fused silica composites have been reported with enhanced properties such as optical, electrical and mechanical properties [17].

Inconsideration of the success associated with the previously published work, attempts have been made in our laboratory to combine the high adsorption capacity of MWCNT with active structural silica by synthesis of multi-wall CNT and silica (MWCNT/SiO_2) nanocomposite. Then, it was characterized and its sorption performance was then tested for sorption of Pb(II) from aqueous solutions. The effects of several operating parameters such as initial Pb(II) concentration, contact time, pH, and temperature were investigated. Kinetic, isotherm and thermodynamic studies were performed.

2. Materials and methods

2.1. Chemicals and materials

Hydrochloric acid, sulphuric acid, nitric acid, ethanol, ethylene glycol, lead nitrate, sodium meta silicate and other chemicals used were obtained from Sigma-Aldrich. The glassware was cleaned by soaking in 10% HNO_3 and rinsing with deionized water. MWCNTs were purchased from Cheap.Tubes.com, with the following specifications: >95% purity; 30–50 nm outer diameter; 5–10 nm inside diameter; 10–20 μm length; 60 m^2/g average specific surface area; >100 S/cm electrical conductivity; 0.28 g/cm^3 bulk density; ~2.1 g/cm^3 true density. The lead ions stock solution (1,000 mg/l) Pb(II) was prepared from lead nitrate (Sigma, purity 99.99%).

2.2. MWCNT functionalization with oxygen containing groups

The pristine MWCNTs were mixed with a solution of concentrated H_2SO_4 and HNO_3 (3:1). The mixture was sonicated for almost 1 h to break down the large aggregates, and helps to disperse the nanotubes. The mixture was refluxed for 8 h at 80°C under stirring. Oxidized-MWCNTs (o-MWCNTs) were extracted and rinsed with deionized water until the pH was approximately 6, then dried at 100°C.

2.3. Synthesis of MWCNT/SiO_2

For the synthesis of MWCNT/SiO_2, typically 1 g of o-MWCNTs were dispersed in 100 mL deionized water and 50 mL ethylene glycol(1,2-Ethanediol) by ultrasonic vibration for 180 min. Then 0.5 M solution of sodium meta silicate was slowly added, at the rate of 1 mL per 2 min, into the dispersed o-MWCNTs under continuous vigorous stirring at room temperature. The slow addition was necessary to obtain good dispersion of silica onto the surface of nanotubes and to allow for its interaction with the active sites on the nanotubes. The resulting mixture was refluxed at 120°C under vigorous stirring for 10 h. The composite was allowed to cool. It was then filtered and washed with distilled water and dried at 100°C. The composite was calcined for 3 h at 320°C [18,19]. The steps of the MWCNT/SiO_2 composite preparation are illustrated

in Fig. 1. The prepared material was characterized using the scanning electron microscope (SEM), elemental dispersive X-ray (EDX) with elemental mapping, transmission electron microscopy (TEM) and Fourier transform infrared spectroscopy (FT-IR).

2.4. Adsorption tests

The adsorption behaviour of MWCNT/SiO_2 nanocomposite was investigated for the removal of Pb (II) from aqueous solutions by batch tests. A predetermined amount, 30 mg, of the adsorbent was added into 20 mL of Pb(II) solution in a plastic container. The containers were placed in a bath shaker at a speed of 150 rpm until the equilibrium was reached. The effect of the temperature was investigated by adjusting the temperature of the bath. The pH value of the medium was adjusted by 2 M hydrochloric acid or sodium hydroxide solutions. Experimental parameters such as effects of pH, initial Pb(II) concentration, contact time and temperature were investigated. The lead-loaded MWCNT/SiO_2 was characterized by SEM/EDX and mapping.

The percentage of removed metal ions in the solution was computed using the following equation:

$$\% \text{ Removal} = \frac{C_0 - C_e}{C_0} \times 100 \quad (1)$$

The amounts of metal adsorbed per unit mass of adsorbent at equilibrium (q_e, mg/g) and at any time t (q_t, mg/g) (adsorption capacity) were calculated from the following equations:

$$q_t = (C_0 - C_e) \times \frac{V}{m} \quad (2)$$

$$q_t = (C_0 - C_t) \times \frac{V}{m} \quad (3)$$

where C_0 (mg/L) is the initial metal concentration, C_e and C_t (mg/L) are the metal concentrations at the equilibrium liquid phase and at any time t, $V(L)$ is the volume of the solution, and m (g) is the mass of adsorbent. The calculated values are based on the results obtained from triplicate determination.

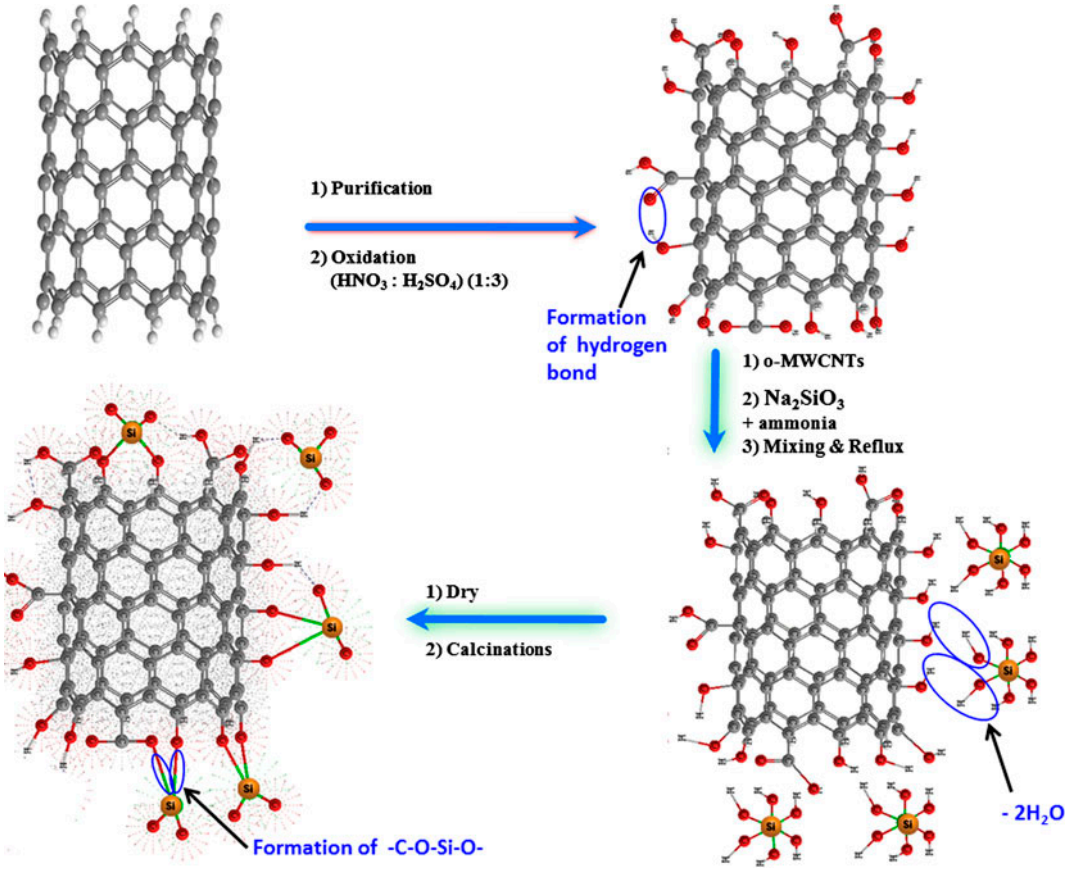

Fig. 1. Schematic illustration of MWCNT/SiO_2 nanocomposite preparation.

3. Results and discussion

3.1. Characterization of MWCNT/SiO_2

SEM and TEM studies: the morphology of the as-synthesized MWCNT/SiO_2 was investigated by field emission scanning electron microscopy (FESEM) and high resolution transmission electron microscopy. The SEM image of MWCNT/SiO_2 nanocomposite is presented in Fig. 2(a) while Fig. 2(b) depicts the HR-SEM image, which clearly indicates silica nanoparticles (nodes) presented on the surface of the nanotubes, see Fig. 2(c), enlarged part of HRSEM. The nodes can be schematically illustrated as shown in Fig. 2(c), where the silica interact with the nanotube via oxygen atoms; –C–O–Si–O–. TEM image, Fig. 2(d), reveals the presence of silica nanoparticles (nodes) on the surface of the nanotubes. The TEM image illustrates the good dispersion of silica nanoparticles on the nanotubes. As shown in the TEM image, the particle size is about 8 nm. This shows that the nanostructure is confirmed.

3.1.1. Brunauer Emmett Teller (BET) surface area analysis

BET surface area analysis was performed using Micromeritics ASAP 2020, and results were interpreted based on the adsorption–desorption of N_2 at 77 K for the CNTs and MWCNT/SiO_2. The BET surface area values obtained for the raw CNTs and MWCNT/SiO_2 were 167.8 and 257.9 m^2/g, respectively.

EDX studies: EDX spectrum of MWCNT/SiO_2 composite is presented in Fig. 2(e). The inset SEM image depicts the areas from which the EDX spectra were taken. The table inset in Fig. 2(e) depicts the elemental analysis, which indicates the presence of carbon, oxygen and silicon elements of 87.85, 10.82, 1.31 wt.%, respectively. Compared with EDX of MWCNT reported earlier [15], the oxygen % in MWCNT/SiO_2 composite is high, due to the large number of oxygen on the silica surface.

FT-IR studies: Fig. 3 presents the FT-IR spectra of SiO_2, MWCNT and MWCNT/SiO_2. The IR spectrum of the pristine MWCNT indicates the characteristic features of the oxygen containing groups; hydroxyl and carboxylic groups. The band at 1,720 $cm^{-1}$is assigned to the stretching vibration of C=O in carboxyl group. The band at 1,650 $cm^{-1}$is assigned to the carbonyl functional group. Spectra shows that a band at 1,580 cm^{-1}corresponds to stretching vibrations of isolated C=C double bonds [18]. A strong band in the C–O stretching region is observed at about 1,180 cm^{-1} (broadband 1,100–1,300 cm^{-1}). Bands at 2,990 and 2,880 cm^{-1} are due to asymmetric and symmetric stretching of CH and indicative of the presence of aliphatic –CH_2 groups.

The IR spectrum of SiO_2 depicted in Fig. 3 shows the characteristic adsorption bands of silicon dioxide, the Si–O–Si asymmetric and symmetric stretching vibration at 1,080 and almost 800 cm^{-1}, respectively, and the O–Si–O symmetric bending vibration at 470 cm^{-1} [20].

The IR spectrum, Fig. 3, of MWCNT/SiO_2 was obtained to further understand the formation of MWCNT/SiO_2. The band at around 470 $cm^{-1}$is assigned to Si–O bond. This absorption band reveals the vibrational properties of Si–O bond (υSi−O), which is obviously caused by the existence of silica on nanotube surface. We can clearly observe that the peaks located between 1,580 and 1,720 cm^{-1} decrease in intensity with the introduction of silica onto nanotubes. Those at around 1,630 cm^{-1} are C=O of stretching vibrational mode. As can be observed, this band has shifted to a lower frequency, which confirms the existence of a close interaction between silica and nanotubes and thus possibly the forming of a chemical bond between silica and nanotubes. It can be proposed that hydrogen bonding occurs with surface hydroxyl functionalities of the silica with carboxylic acid groups, i.e. Si–OH…O=C(OH)—nanotube, followed by removal of the H_2O molecule.

Therefore, carboxylic groups on the nanotubes and hydroxylic groups of the silica interact with each other via esterification. The three possible structures are monodentate (i), bidentate bridging (ii) and bidentate chelating (iii). During the hydrothermal process, the ester bonds and a –C–O–Si bonds are formed and a number of hydroxyl groups on silica surface can be generated. It was observed that silica nanoparticles (nodes) attached on the nanotubes did not fall off even after washing and sonication for 2 d, as confirmed by TEM image, indicating strong interaction between silica and nanotubes.

Thus, directed by the SEM, TEM, EDX, elemental mapping and FTIR studies, we univocally conclude the successful realization of MWCNT/SiO_2 nanostructure. Therefore, it can be proposed that carboxylic groups on the nanotubes and hydroxylic groups of the silica interact with each other via esterification. The three possible structures are monodentate (i), bidentate bridging (ii) and bidentate chelating (iii) proposed in Fig. 4. During the hydrothermal process, the ester bonds and a –C–O–Si bonds are formed and a number of hydroxyl groups on silica surface can be generated. It was practically observed that silica nanoparticles (nodes) attached on the nanotubes did not fall off even after washing and sonication for a long time, 2 d, as it was then confirmed by TEM image, which also

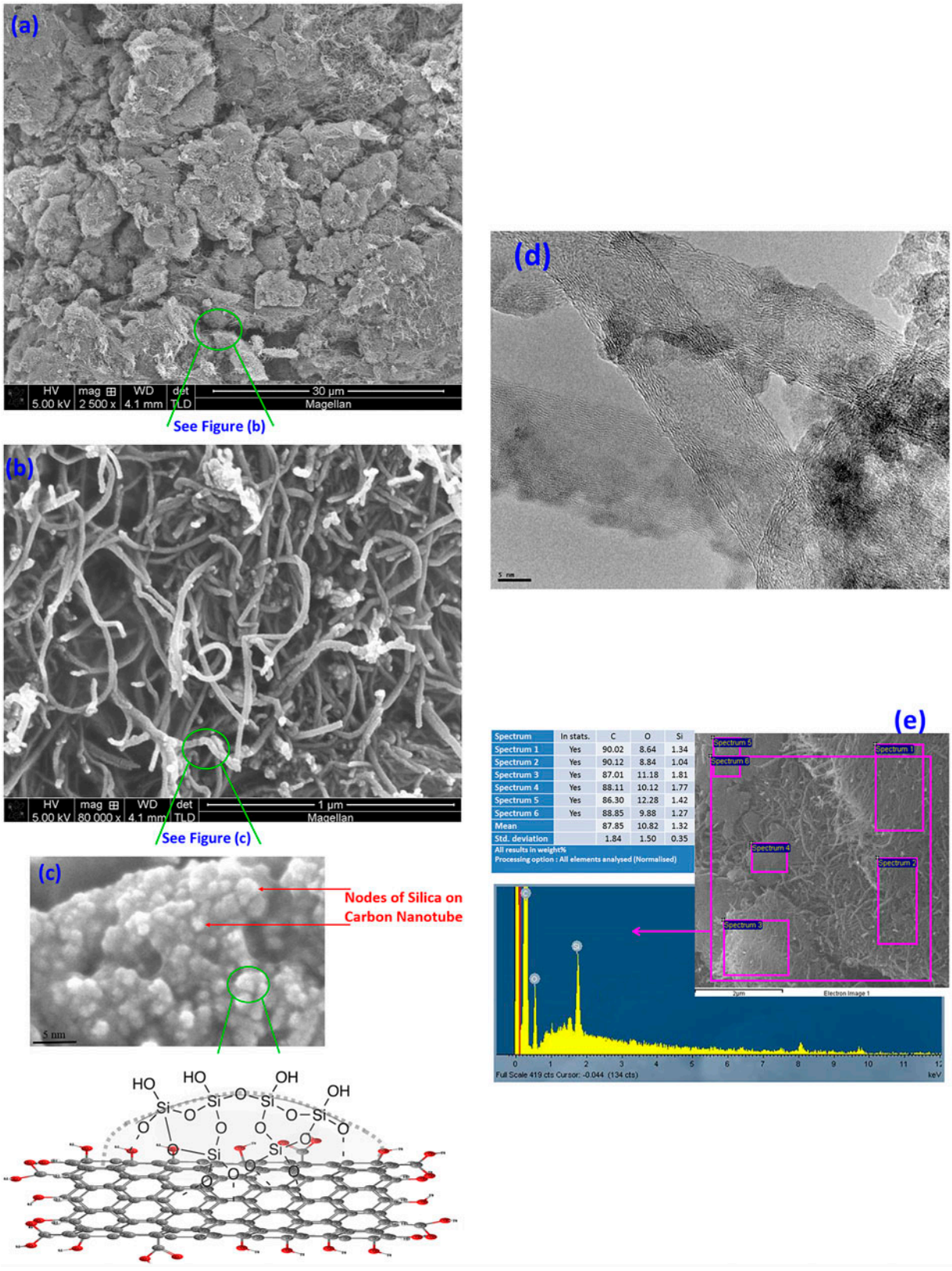

Fig. 2. FESEM image (a), HR-SEM image (b), enlarged part of HRSEM with a representative scheme of the nodes of silica on carbon nanotubes (c), TEM image (d) and EDX analysis (e) of MWCNT/SiO_2.

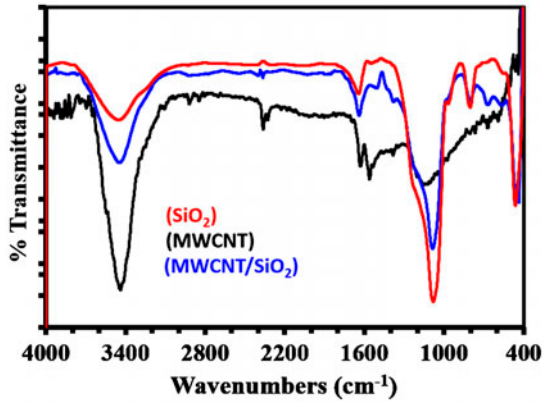

Fig. 3. FT-IR spectrum of SiO_2, MWCNT and MWCNT/SiO_2.

indicates possible strong interaction between silica and nanotubes.

3.2. Sorption evaluation for lead(II) removal

Heavy metal wastewater poses a pervasive threat to the environment. In this context, to explore the worth of the MWCNT/SiO_2, we have performed the sorption tests using the aqueous solution of lead(II). *Comparison*: A comparison study was conducted to evaluate the adsorption performance of MWCNT/SiO_2 compared with MWCNTs and silica nanoparticles, Fig. 5. Silica nanoparticles were prepared by sol–gel process reported by Rao et al. [21]. Briefly, tetraethyl orthosilicate was added into ethanol while sonicating. After 20 min, 28% ammonium hydroxide was added to promote the condensation reaction. The mixture was kept under sonication for 1 h to get a white turbid suspension. The maximum adsorption percentage was observed on MWCNT/SiO_2 (~95%) followed by silica nanoparticles (~50%) and MWCNTs (~45%). This may be due to the availability of large adsorption sites on the composite compared to silica and pristine nanotubes. It should be mentioned that the optimum MWCNT: SiO_2 ratio was found to be 5% MWCNT. This mixture was observed to have the higher adsorption.

pH Effect on Pb(II) adsorption: The pH value of initial solution of Pb(II) is considered as an important parameter in the adsorption process that significantly affects the surface charge, the protonation degree of the adsorbent and the conversion of lead species. Pb (II) speciation is related to the pH value of the solution [22]. The pH of the initial solutions was varied between 2.0 and 7.0. A solution of pH >7 was not examined to avoid metal ion precipitation. Adsorption of Pb(II) on MWCNT/SiO_2 as a function of pH is shown in Fig. 6(a), which indicates the maximum percentage removal achieved at a range of pH 5–7, which is consistent with the previous studies [23].

pH_{pzc} of MWCNT/SiO_2 and lead speciation are used to explain the pH effect. According to the lead speciation diagram [24], the Pb(II) exists in various forms; Pb^{2+} at pH value ≤7, $Pb(OH)^+$ at pH value ≥ 7 ≤ 9, $Pb(OH)_2$at pH value between 9 and 11 and

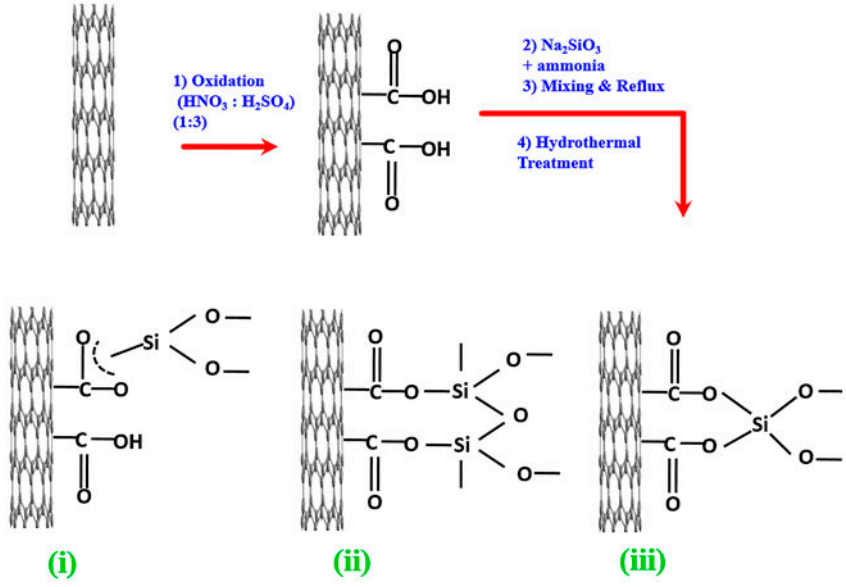

Fig. 4. The possible structures between carbon nanotubes-carboxylate and silica.

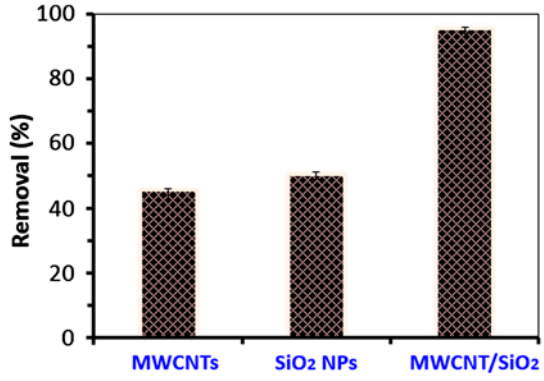

Fig. 5. Comparison between MWCNTs, silica nanoparticles and MWCNT/SiO_2 for the adsorption of Pb(II) under the same experimental conditions.

$Pb(OH)_3^-$ at pH values ≥11. The point of zero charge of the MWCNT/SiO_2 was determined to be 4, Fig. 6(b). Thus, at pH ≤ 4, the surface of the nanocomposite is relatively positive due to protonation, so the interaction or adsorption of Pb^{2+} at pH value ≤4 is hindered by the repulsion as H^+ competes with Pb^{2+}. However, solutions of pH value >4, the surface of the nanocomposite is negative due to deprotonation, and the lead is in form of Pb^{2+} so the adsorption of Pb^{2+} at this pH range is enhanced by interaction between the negative charged adsorbent surfaces and the dipositive lead ions. Thus, at pH of a range between 5 and 7, the lead species is Pb^{2+} and the removal of Pb is accomplished by sorption. According to the lead speciation, lead is in $Pb(OH)^+$ form at pH value ≥ 7 ≤ 9, thus lead removal can be accomplished by concomitant precipitation of $Pb(OH)_2$ and sorption of $Pb(OH)^+$. Therefore, to ensure a quantitative sorption and avoid metal ion hydrolysis at higher pH, a pH of 6 was chosen as optimum.

Effect of contact time and initial concentration: The effect of contact time on the adsorption of Pb(II) was investigated for an initial concentration of 5, 10 and 30 ppm in batch experimental mode. The contact time experiments were performed at room temperature ≈22°C. The effect of contact time on the adsorption of Pb(II) onto MWCNT/SiO_2 is shown in Fig. 6(c). The fast adsorption of Pb(II) ions at the initial stages can be explained by availability of the uncovered surface and active sites on the nanocomposite. The adsorption increased with increasing contact time till equilibrium was attained. The removal percentage of Pb(II) increases continuously until the contact time reaches 50, 90 and 100 min for the concentration of 5, 10 and 30 ppm, respectively. Increasing the contact time beyond these limits has no considerable enhancement

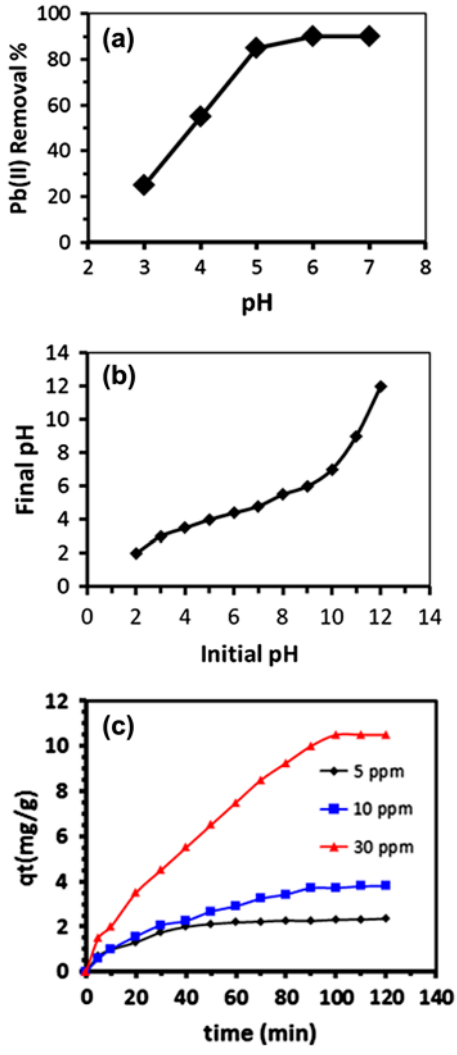

Fig. 6. Effect of pH on the adsorption of Pb(II) ions (a); point of zero net proton charge (b); the variation of adsorption q_t with adsorption time for adsorption of Pb(II) on MWCNT/SiO_2 for different initial feed concentration (c).

on the adsorption percentage since the systems reached the equilibrium.

The amount of Pb(II) adsorbed on the nanocomposite, q_e (mg/g), increased with increasing the initial concentration. At equilibrium, the amount of Pb(II) adsorbed onto MWCNT/SiO_2 increased from approximately 2.7 to 10.5 mg/g, and the percentage removal was decreased from 90 to 70% with the increase in the initial concentration from 5 to 30 ppm.

At low concentrations, the ratio of available surface to initial Pb(II) concentration was larger than the ratio at high initial concentrations. The percentage removal then depended upon the initial concentration. The results indicate that the percentage adsorption decreased by increasing the initial concentration.

3.3. Adsorption kinetic study

The adsorption kinetics are useful for adsorption studies to predict the rate at which Pb(II) is removed from aqueous solutions and provide valuable data for understanding the mechanism of sorption and the reaction pathways. Two kinetic models (Lagergren's pseudo-first order and pseudo-second order) were employed to investigate the mechanisms of Pb(II) adsorption on MWCNT/SiO_2. The conformity between experimental results and the model predicted values can be expressed by the correlation coefficients (R^2). Relatively high correlation coefficients indicated that the model successfully describes the kinetics of the adsorption.

Lagergren's pseudo-first order: The equation for pseudo-first order kinetics is presented as follows [25]:

$$\ln (q_e - q_t) = \ln q_e - k_1 t \tag{4}$$

where q_t and q_e are the amounts of Pb(II) (mg/g) adsorbed at time t and at equilibrium, respectively. k_1 is the rate constant of the pseudo-first order adsorption process (min^{-1}). The values of k_1 and adsorption density q_e are calculated from the slope and intercept of plots of ln ($q_e - q_t$) vs. t (Fig. 7(a)) and presented in Table 1. Comparing the experimental observed equilibrium adsorption ($q_{e,exp}$) and that calculated theoretically ($q_{e,cal}$), it is clear that there is no agreement between the values. The correlation coefficients (R^2) for the pseudo-first order model obtained at 5, 10 and 30 ppm were low, showing poor linearity. This assumed that the adsorption of Pb(II) deviated from the Lagergren's pseudo-first order kinetic model, which indicates that this model is not useful for explaining the adsorption mechanism of Pb(II) on the nanocomposite.

The pseudo-second order kinetic model is expressed by the following adsorption kinetic rate equation [26]:

$$\frac{dq_t}{dt} = k_2 (q_e - q_t)^2 \tag{5}$$

where k_2 is the rate constant of the pseudo-second order adsorption (g/mg min), q_e and q_t are the adsorbed amount (capacity) of Pb(II) at equilibrium and time t, respectively. The value of k_2 often depends on the applied operating conditions, such as initial metal concentration, pH of solution, temperature and agitation rate. For the boundary conditions applied from $t = 0$ to $t = t$ and $q_t = 0$ to $q_t = q_e$, the Eq. (4) after the integration becomes:

$$\frac{1}{q_e - q_t} = \frac{1}{q_e} + k_2 t \tag{6}$$

Eq. (5) represents the integrated rate law for pseudo-second order and can be expressed in the linear form as:

$$\frac{t}{q_t} = \frac{1}{k_2 q_e^2} + \frac{t}{q_e} \tag{7}$$

where k_2, the rate constant (g/mg min), is obtained by a plot of t/q_t against t (Fig. 7(b)). All the kinetic parameters are listed in Table 1. The initial adsorption rate: $h = k_2 q_e^2$ (mg/g min).

The results obtained from the correlation coefficients ($R^2 > 0.99$) for all concentrations indicates that the adsorption process follows the pseudo-second order kinetic model, and Pb(II) ions were adsorbed on the surface of MWCNT/SiO_2 via chemical interaction. This is supported by the close agreement of the equilibrium adsorption capacities ($q_{e,cal}$) derived from Eq. (7) with the experimentally observed data ($q_{e,exp}$). Other workers in adsorption of Pb(II) also observed similar phenomena [4].

The intraparticle diffusion model: The commonly used model to identify the mechanism involved in the adsorption is the intraparticle diffusion technique. In an agitated batch adsorption system, there is a possibility of intraparticle pore diffusion of adsorbate ions, which can be the rate-limiting step. A plot of q_t vs. $t^{0.5}$ should be a straight line when the mechanism of the adsorption follows the intraparticle diffusion process. However, if the data exhibit multi-linear plots, two or more steps govern the process. There are two or more consecutive steps involved in the adsorption of an adsorbate by adsorbent. In step one (called surface diffusion) the sorbate molecules are transported from the solutions to the external surfaces of the adsorbent. In step two (called intraparticle or pore-diffusion), the sorbate molecule moves into the interior of sorbent particles. The third step involved the adsorption of the sorbate molecule onto the interior sites of the sorbent. The intraparticle diffusion coefficient, k_{id}, can be determined by fitting the experimental data in the intraparticle diffusion model [27] expressed as:

$$q_t = k_{id} t^{1/2} + C \tag{8}$$

where k_{id} is the intraparticle diffusion rate constant (mg/g $min^{½}$), and C is the intercept (mg/g). According to this model, the linearity of the plot indicates that intraparticle diffusion is involved in the

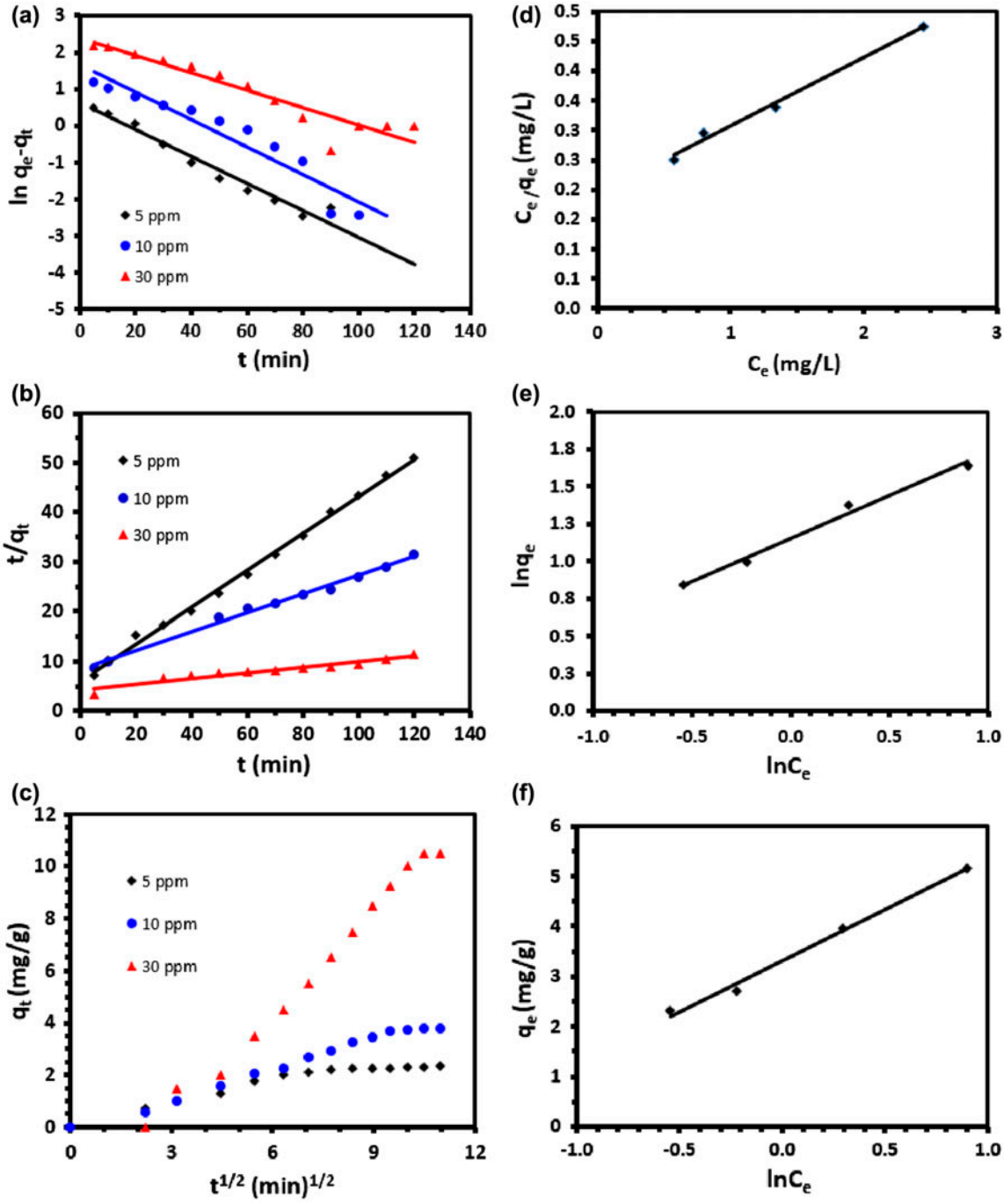

Fig. 7. Lagergren first-order (a), pseudo-second order (b), intraparticle diffusion (c), kinetic plots for Pb(II) adsorption; Langmuir (d), Freundlich (e) and Temkin (f) adsorption isotherms.

adsorption process. When the line passes through the origin then intraparticle diffusion is the rate-controlling step. When the plot does not pass through the origin then it indicates some degree of boundary layer control and the intraparticle diffusion is not the only rate-limiting step, but also other kinetic models may control the rate of adsorption.

Experimental data for the adsorption of Pb(II) onto MWCNT/SiO_2 were examined by the intraparticle diffusion model to identify the mechanism involved in the adsorption process. Fig. 7(c) revealed that the plot of q_t vs. $t^{1/2}$ were multi-linear, indicating that more than one step is involved in the adsorption process [28]. It is observed that there are three linear portions,

Table 1
Kinetic constant parameters obtained for Pb(II) adsorption on the surface of MWCNT/SiO_2; the comparison between the experimental adsorption capacity (q_{exp}) and the calculated ones (q_{cal}); the linear correlation coefficient values

C_i (mg/L)	$q_{e,exp}$ (mg/g)	Lagergren's pseudo-first order			Pseudo-second order			Intraparticle diffusion model		
		k_1 (min^{-1})	$q_{e,cal}$ (mg/g)	R^2	k_2 (g/mg min)	q_e, cal (mg/g)	R^2	k_{id} (mg/g min)	C (mg/g)	R^2
5	2.4	0.034	1.85	0.97	0.048	2.68	0.99	0.42	2.62	0.98
10	4.8	0.037	5.28	0.94	0.004	5.2	0.99	0.77	4.88	0.98
30	10.5	0.023	10.5	0.94	0.0018	11.3	0.99	1.04	7.33	0.99

which elucidate the adsorption stages: external mass transfer at initial period followed by intraparticle diffusion of Pb(II) on MWCNT/SiO_2; adsorption on the interior sites. The slope of the second linear portion, the rate of intraparticle diffusion (k_{id}), increases with increasing initial concentration. The intraparticle diffusion constant values are shown in Table 1.

3.4. Adsorption isotherms

Langmuir isotherm model: introduced a concept of forming a monolayer surface phase (a monomolecular adsorption) on energetically homogeneous surfaces of the adsorbent. Thus, the Langmuir equation describes relatively well physical or chemical adsorption on solid surfaces with one type of adsorption active centre [29]. This is called ideal localized monolayer model.

The linear Langmuir equation is given by:

$$\frac{C_e}{q_e} = \frac{1}{K_L q_m} + \frac{C_e}{q_m} \tag{9}$$

where K_L is Langmuir equilibrium constant (litres/milligrams) related to the affinity of adsorption sites, and q_m (mg/g) is the maximum theoretical monolayer adsorption capacity, C_e is the equilibrium concentration (mg/L = ppm) of Pb(II) in solution and q_e is the amount of Pb(II) ions adsorbed (mg/g) at equilibrium. Fig. 7(d) depicts the plot of C_e/q_e vs. C_e.

The values of Langmuir constants q_m and K_L were computed from the slope and intercept of the plot, and are given in Table 2 along with correlation coefficient (R^2). From the data of this research work, the adsorption capacity q_m was determined by linear Langmuir equation to be 13 mg/g of Pb(II) on MWCNT/SiO_2, K_L of 0.4 L/mg, the R^2 value of 0.99 proving that the sorption data fitted well to the Langmuir Isotherm model.

The characteristic parameter of Langmuir isotherm can be illustrated in terms of dimensionless equilibrium parameter R_L, also known as separation factor, defined by Weber and Chakkravorti [27]:

$$R_L = \frac{1}{1 + K_L C_o} \tag{10}$$

where C_o is the initial solute concentration. The value R_L gives an indication of the type of the isotherm and the nature of the adsorption process. It indicates the adsorption nature to be either unfavourable ($R_L > 1$), linear ($R_L = 1$), favourable ($0 < R_L < 1$) and irreversible (R_L is zero). From the data calculated in Table 2, the R_L of 0.3 indicates that the adsorption nature is favourable.

The maximum monolayer adsorption capacities from Langmuir isotherm of MWCNT/SiO_2 for the removal of Pb(II) was compared with those of other adsorbents reported in the literature. It is clear from Table 3 that the adsorption capacity of MWCNT/SiO_2 was comparable to the previously reported capacities.

Freundlich Isotherm Model: The Freundlich model is used to describe the adsorption characteristics for the heterogeneous surface [27]. Freundlich equations were derived as the overall adsorption isotherms for

Table 2
Langmuir, Freundlich and Temkin isotherms constant for Pb(II) adsorption on the surface of MWCNT/SiO_2

Langmuir isotherm				Freundlich isotherm				Temkin isotherm		
q_m (mg/g)	K_L (L/mg)	R_L	R^2	$1/n$	n	K_F (mg/g)	R^2	K_T (L/g)	b_T (kJ/mol)	R^2
13.23	0.4	0.3	0.99	0.57	1.75	3.16	0.98	5.08	1.213	0.99

Table 3
Comparing the adsorption capacity of MWCNT/SiO_2 with the adsorption capacity of different adsorbents for Pb(II)

Adsorbents capacity	(mg/g)	Refs.
Commercial silica	3.9	[30]
Initial MWCNTs	4	[31]
Zeolites: chabazite	6.0	[32]
Zeolites: clinoptilolite	1.6	[33]
Manganese oxide-coated zeolite	1.117	[34]
Activated carbon	6.68	[35]
Rolling mill scale	2.74	[36]
Periwinkle shell carbon	0.0558	[37]
Baggase fly ash	2.5	[38]
MWCNT/SiO_2 nanocomposite	13	This work

adsorption on heterogeneous solid surfaces, and the interactions between the adsorbed molecules were taken into account. The model of heterogeneous solids assumes a definite distribution of adsorption sites on the surface. The following empirical equation is used:

$$q_e = K_F C_e^{\frac{1}{n}} \tag{11}$$

where K_F (mg/g) is the Freundlich isotherm constant indicating adsorption capacity and n is adsorption intensity while $1/n$ is a function of the strength of the adsorption, C_e is the equilibrium concentration of adsorbate (mg/L) and q_e is the amount of metal adsorbed per gram of the adsorbent at equilibrium (mg/g). The logarithmic form of the Freundlich model is defined by the following equation:

$$\ln\ q_e = \ln\ K_F + \frac{1}{n}\ \ln\ C_e \tag{12}$$

From the slope and intercept of the straight portion of the linear plot ln q_e vs. ln C_e, Fig. 7(e), K_F and n were calculated, Table 2. The n value gives an indication of the favourability of the adsorption process. The values of $n > 1$ represent favourable adsorption condition. If $n = 1$, then the partition between the two phases are independent of the concentration. The value of $1/n < 1$ indicates a normal adsorption while $1/n > 1$ indicates a cooperative adsorption. Here, in this study the value of $1/n$ is 0.6, indicating a favourable adsorption process of Pb(II) on MWCNT/SiO_2. The value of R^2 is 0.98 and K_F is 3 mg/g.

Temkin Isotherm Model: It takes explicitly into the account the adsorbent–adsorbate interactions. The Temkin model assumes that the adsorption energy (the heat of adsorption of all the molecules in a layer) decreases linearly with the surface coverage due to adsorbent–adsorbate interactions. It also assumes that the adsorption is characterized by a uniform distribution of the bonding energies up to some maximum binding energy. The linear form of the Temkin isotherm model is expressed by:

$$q_e = \frac{RT}{b_T}\ \ln\ K_T + \frac{RT}{b_T}\ \ln\ C_e \tag{13}$$

where b_T is the Temkin isotherm constant related to the heat of sorption (joule per mole), K_T is the Temkin isotherm equilibrium binding constant (L/g) which is equal to the maximum binding energy (L/g), R is gas constant (8.314×10^{-3} kJ/mol K) and T is the absolute temperature [39].

$$B = \frac{RT}{b_T} \tag{14}$$

B is considered as a constant related to the heat of sorption (J/mol). The plot of q_e vs. ln C_e is illustrated in Fig. 7(f). The isotherm constants were determined from the slope and intercept. The linear plot for Temkin adsorption isotherm fits quite well with correlation coefficient R^2 of 0.99. Thus, the adsorption of Pb(II) on MWCNT/SiO_2 is a chemisorption process [40].

3.5. Thermodynamic parameters

The thermodynamic parameters such as ΔG° (standard free energy), ΔH° (enthalpy change) and ΔS° (entropy change) have been estimated to determine the feasibility and nature of the adsorption process. The experimental data obtained at different temperatures were used for calculating the thermodynamic parameters. The values of ΔH° and ΔS° were calculated from the slopes and intercepts of the plots of ln K_c vs. $1/T$, for adsorption of Pb(II) on MWCNT/SiO_2, by using the following linear Van't Hoff equation.

$$\ln\ K_c = \frac{\Delta S^0}{R} - \frac{\Delta H^0}{RT} \tag{15}$$

Table 4
Thermodynamic parameters for the adsorption of Pb(II) on MWCNT/SiO_2 at different temperatures

T (K)	ΔG° (kJ/mol)	ΔH° (kJ/mol)	ΔS° (kJ/mol K)
295	−5.02	29.4	0.1168
315	−7.36		
335	−9.71		

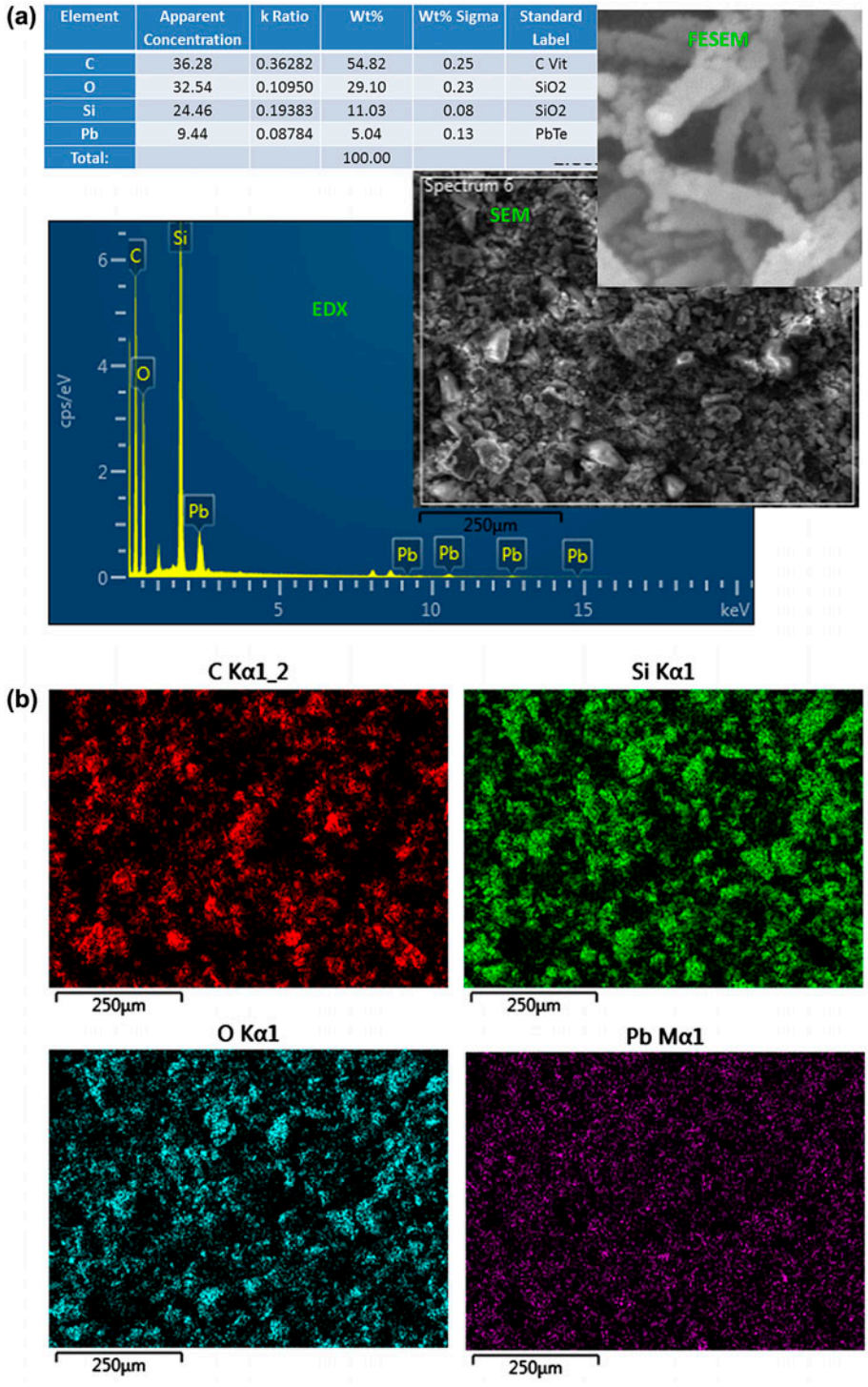

Fig. 8. (a) EDX spectrum and the corresponding SEM image of lead-loaded MWCNT/SiO_2, the inset presents the FESEM image, the table shows the elemental analysis of the sample; (b) elemental mapping image of lead-loaded MWCNT/SiO_2.

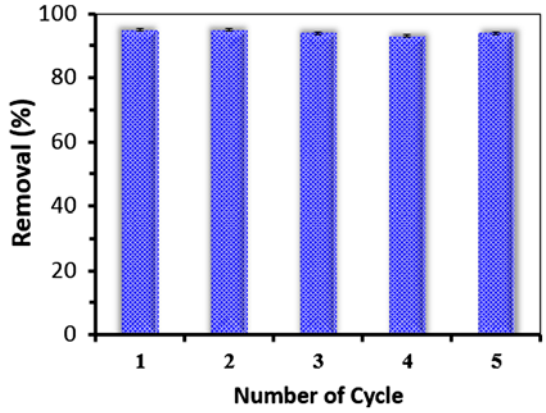

Fig. 9. Adsorption/desorption and repeated cycles by MWCNT/SiO_2.

The ΔG° (free energy change) was calculated from the following equation:

$$\Delta G^{o} = \Delta H^{o} - T\Delta S^{o} \quad (16)$$

where R (8.314 kJ/mol K) is the gas constant, T (K) is the absolute temperature and K_c (L/mg) is the standard thermodynamic equilibrium constant defined by q_e/C_e.

The decrease in ΔG° value with increasing temperature reveals that adsorption of the ion on the adsorbent becomes favourable at higher temperature. The positive standard enthalpy change ΔH° of 29 kJ/mol suggests the adsorption of Pb(II) by MWCNT/SiO_2 is endothermic, i.e. supported by the increasing adsorption of Pb(II) with the increase in temperature. The positive standard entropy change (116.8 J mol^{-1} K^{-1}), Table 4, reflects the affinity of the nanocomposite towards Pb(II). It also reveals the increase in randomness at solid solution interface during the fixation of Pb(II) on the active sites.

Adsorption activation energy: The adsorption activation energy is computed from the rate constant (k_2) obtained from the pseudo-second order kinetic model using the Arrhenius equation expressed as:

$$\ln k_2 = -\frac{E_a}{R}\left(\frac{1}{T}\right) + \text{constant} \quad (17)$$

where k_2 is the pseudo-second order rate constant in g/mg h, E_a is the activation energy (kJ/mol), R is the universal gas constant (8.314 J/mol K) and T is the solution temperature (K). The constant in the equation is considered to be $\ln A$, where A is the Arrhenius temperature independent factor. The magnitude of E_a gives an indication of a type of adsorption; physical or chemical process. The physisorption process is readily reversible, equilibrium is attained rapidly and thus energy requirements are small, ranging between 5 and 40 kJ/mol. The chemisorption mechanism is specific and involves stronger forces and thus requires large activation energy ranging from 40 to 800 kJ/mol [41]. In this study, the calculated value of apparent activation energy E_a was 15.8 kJ/mol assuming the adsorption has a low potential barrier and is assigned to a physical sorption.

SEM/EDX analysis after adsorption: Energy dispersive X-ray (EDX) analysis was conducted to examine the adsorption of Pb(II) on MWCNT/SiO_2. The EDX spectrum recorded for Pb(II)-loaded MWCNT/SiO_2 gives the characteristic peaks for Pb(II) at 2.34 and 10.55 keV in addition to the peaks of carbon at 0.277, oxygen at 0.525 and silica at 1.74. This confirms the

Table 5
Comparison of Pb(II) concentrations in wastewater sample before and after the treatment with the nanocomposite

		After treatment (μg L^{-1}) Original sample spiked with Pb^{2+} ions and then treated with the nanocomposite under optimum conditions		
Metal	Original sample (μg L^{-1})	0	2,000 (μg L^{-1})	10,000 (μg L^{-1})
Cd	0.48	<MDL	<MDL	0.058
Co	0.262	<MDL	<MDL	<MDL
Cu	28.14	1.20	1.84	1.12
Zn	10.4	0.018	0.241	1.58
As	7.14	<MDL	<MDL	<MDL
Mo	11.72	5.64	5.68	5.85
Sb	<0.031	<MDL	<MDL	<MDL
Pb	0.852	<MDL	0.274	34.65

MDL: the method detection limit.

binding of Pb(II) to the surface of MWCNT/SiO_2. A SEM at 20 kV was used to examine the surface morphologies of Pb(II)-loaded MWCNT/SiO_2. The morphology of the Pb(II)-loaded MWCNT/SiO_2 is shown in the corresponding SEM image in Fig. 8. The FESEM indicates the intact with the nanocomposite structure.

The table (inset, Fig. 8(a)) indicates the apparent concentration or the uncorrected concentration and the element weight per cent for all the elements present in the sample after adsorption, resulting in a total of 100 wt.%. Fig. 8(b) depicts information on the mapping analysis of elements of MWCNT/SiO_2 loaded with lead ions energy. The analysis indicates the coexistence of Si, C, O and lead elements. The distribution of all the elements seems to be homogeneous.

3.6. Desorption studies (reusability)

Reusability of the adsorbent is important in economic development because disposal of the exhausted adsorbent loaded with heavy metal ions creates environmental problems. Thus, regeneration must produce a small volume of metal concentrate suitable for metal recovery without damaging the adsorbent capacity. In our work, to obtain the reusability of the MWCNT/SiO_2, the adsorption followed by desorption cycle was repeated five times with the same adsorbent. The MWCNT/SiO_2 showed high recovery with approximately stable efficiency, Fig. 9. This shows that the MWCNT/SiO_2 is highly effective for the adsorption of Pb(II) ions from aqueous solutions.

3.7. Treatment of real wastewater samples

The industrial wastewater was used to study the effect of real water matrix and to evaluate practical application of MWCNT/SiO_2. The samples were spiked with 0.0, 2.0 and 10 ppm Pb(II), and then treated with MWCNT/SiO_2 under the optimum conditions. The results given in Table 5 indicates that the removal efficiencies of Pb(II) are hardly influenced by the real wastewater matrix. This indicates the high efficiency and capability of MWCNT/SiO_2 to be regarded as a potential adsorbent for high efficient and renewable adsorbent for Pb(II) ions from aqueous solutions.

4. Conclusions

The results obtained confirm that MWCNT/SiO_2 nanocomposite was successfully prepared and can remove Pb(II) ion from aqueous solutions. The optimum pH value for Pb(II) removal was 5–6. The contact time has an effect upon Pb^{2+} adsorption. The linearity of the plots t/q_t vs. t implies the adsorption followed by the pseudo-second order rate kinetics with adsorption capacity of 13 mg/g. Fitting the data to Langmuir, Freundlich and Temkin models shows that the Langmuir and Temkin models give a better correlation coefficient with R^2 of 0.99. The finding confirms that intraparticle diffusion is involved in the adsorption process though it is not the sole rate-controlling step; and some other mechanisms may play an important role. Thermodynamic parameters were evaluated; the negative values of ΔG° indicate the spontaneity and the positive values of ΔH° (29.4 kJ/mol) showed the endothermic nature of Pb(II) sorption on the nanocomposite. The material showed efficient stability and regeneration. Therefore, the nanocomposite could be considered as a potential adsorbent of high efficiency for Pb(II) removal.

Acknowledgements

The support by the Chemistry Department and King Fahd University of Petroleum and Minerals is gratefully acknowledged. The author would like to acknowledge the support provided by the Deanship of Scientific Research (DSR) at King Fahd University of Petroleum & Minerals (KFUPM) for funding this work through project No. JF121009.

References

[1] M.J. Santos Yabe, E. de Oliveira, Heavy metals removal in industrial effluents by sequential adsorbent treatment, Adv. Environ. Res. 7 (2003) 263–272.
[2] M. Ghasemi, M. Naushad, N. Ghasemi, Y. Khosravifard, Adsorption of Pb(II) from aqueous solution using new adsorbents prepared from agricultural waste: Adsorption isotherm and kinetic studies, J. Ind. Eng. Chem. 20 (2014) 2193–2199.
[3] EPA (Environmental Protection Agency), Environmental Pollution Control Alternatives, EPA/625/5-90/025, EPA/625/4-89/023, Environmental Protection Agency, Cincinnati, 1990.
[4] M. Jiang, Q. Wang, X. Jin, Z. Chen, Removal of Pb(II) from aqueous solution using modified and unmodified kaolinite clay, J. Hazard. Mater. 170 (2009) 332–339.
[5] T.A. Saleh, V.K. Gupta, Processing methods, characteristics and adsorption behavior of tire derived carbons: A review, Adv. Colloid Interface Sci. 211 (2014) 93–101.
[6] M.M. Rao, D. Ramana, K. Seshaiah, M. Wang, S. Chien, Removal of some metal ions by activated carbon prepared from *Phaseolus aureus* hulls, J. Hazard. Mater. 166 (2009) 1006–1013.
[7] J.M. Dias, M. Alvim-Ferraz, M.F. Almeida, J. Rivera-Utrilla, M. Sánchez-Polo, Waste materials for activated carbon preparation and its use in aqueous-phase treatment: A review, J. Environ. Manage. 85 (2007) 833–846.

[8] K.G. Bhattacharyya, S.S. Sen Gupta, Pb(II) uptake by kaolinite and montmorillonite in aqueous medium: Influence of acid activation of the clays, Colloids Surf., A 277 (2006) 191–200.
[9] E. Erdem, N. Karapinar, R. Donat, The removal of heavy metal cations by natural zeolites, J. Colloid Interface Sci. 280 (2004) 309–314.
[10] Q. Chen, C.D. Hills, M. Yuan, H. Liu, M. Tyrer, Characterization of carbonated tricalcium silicate and its sorption capacity for heavy metals: A micron-scale composite adsorbent of active silicate gel and calcite, J. Hazard. Mater. 153 (2008) 775–783.
[11] S. Pacheco, J. Tapia, M. Medina, R. Rodriguez, Cadmium ions adsorption in simulated wastewater using structured alumina–silica nanoparticles, J. Non-Cryst. Solids 352 (2006) 547–55481.
[12] P. Yin, Q. Xu, R. Qu, G. Zhao, Y. Sun, Adsorption of transition metal ions from aqueous solutions onto a novel silica gel matrix inorganic–organic composite material, J. Hazard. Mater. 173 (2010) 710–716.
[13] S. Iijima, Helical microtubules of graphitic carbon, Nature 354 (1991) 56–58.
[14] S. Anna, P. Krystyna, Adsorption of heavy metal ions with carbon nanotubes, Sep. Purif. Technol. 58 (2007) 49–52.
[15] T.A. Saleh, The influence of treatment temperature on the acidity of MWCNT oxidized by HNO_3 or a mixture of HNO_3/H_2SO_4, Appl. Surf. Sci. 257(17) (2011) 7746–7751.
[16] H. Liu, J. Li, X. Liu, S. Jiang, A novel multiwalled carbon nanotubes bonded fused-silica fiber for solid phase microextraction–gas chromatographic analysis of phenols in water samples, Talanta 78 (2009) 929–935.
[17] C.S. Xiang, Y.B. Pan, X.J. Liu, X.M. Shi, X.W. Sun, J.K. Guo, Electrical properties of multiwalled carbon nanotube reinforced fused silica composites, J. Nanosci. Nanotechnol. 6 (2006) 3835–3841.
[18] T.A. Saleh, V.K. Gupta, Functionalization of tungsten oxide into MWCNT and its application for sunlight-induced degradation of rhodamine B, J. Colloid Interface Sci. 362(2) (2011) 337–344.
[19] M.T. Martínez, M.A. Callejas, A.M. Benito, M. Cochet, T. Seeger, A. Anson, J. Schreiber, C. Gordon, C. Marhic, O. Chauvet, J.L.G. Fierro, W.K. Maser, Sensitivity of single wall carbon nanotubes to oxidative processing: Structural modification, intercalation and functionalisation, Carbon 41 (2003) 2247–2256.
[20] N.E.A. El-Gamel, L. Wortmann, K. Arroub, S. Mathur, $SiO_2@Fe_2O_3$ core–shell nanoparticles for covalent immobilization and release of sparfloxacin drug, Chem. Commun. 47 (2011) 10076–10078.
[21] K.S. Rao, K. El-Hami, T. Kodaki, K. Matsushige, K. Makino, A novel method for synthesis of silica nanoparticles, J. Colloid Interface Sci. 289 (2005) 125–131.
[22] T.A. Saleh, V.K. Gupta, A.A. Al-Saadi, Adsorption of lead ions from aqueous solution using porous carbon derived from rubber tires: Experimental and computational study, J. Colloid Interface Sci. 396 (2013) 264–269.
[23] N. Bensacia, I. Fechete, S. Moulay, O. Hulea, A. Boos, F. Garin, Kinetic and equilibrium studies of lead(II) adsorption from aqueous media by KIT-6 mesoporous silica functionalized with –COOH, C.R. Chim. 17 (2014) 869–880.
[24] V.K. Gupta, S. Agarwal, T.A. Saleh, Synthesis and characterization of alumina-coated carbon nanotubes and their application for lead removal, J. Hazard. Mater. 185(1) (2011) 17–23.
[25] S. Lagergren, About the theory of so-called adsorption of solution substances, Kunglia Srenska Vertens Ka Psakademiens Handlingar. 24 (1898) 1–39.
[26] Y.S. Ho, Review of second-order models for adsorption systems, J. Hazard. Mater. 136 (2006) 681–689.
[27] T.N. Weber, R.K. Chakravorti, Pore and solid diffusion models for fixed-bed adsorbers, AIChE J. 20 (1974) 228–238.
[28] G. Annadurai, R.S. Juang, D.J. Lee, Use of cellulose-based wastes for adsorption of dyes from aqueous solutions, J. Hazard. Mater. 92 (2002) 263–274.
[29] I. Langmuir, The adsorption of gases on plane surfaces of glass, mica and platinum, J. Am. Chem. Soc. 40 (1918) 1362–1403.
[30] N. Chiron, R. Guilet, E. Deydier, Adsorption of Cu(II) and Pb(II) onto a grafted silica: Isotherms and kinetic models, Water Res. 37 (2003) 3079–3086.
[31] H.J. Wang, A.L. Zhou, F. Peng, H. Yu, L.F. Chen, Adsorption characteristic of acidified carbon nanotubes for heavy metal Pb(II) in aqueous solution, Mater. Sci. Eng., A 466 (2007) 201–206.
[32] S.K. Ouki, M. Kavannagh, Performance of natural zeolites for the treatment of mixed metal-contaminated effluents, Waste Manage. Res. 15 (1997) 383–394.
[33] M.J. Zamzow, B.R. Eichbaum, K.R. Sandgren, D.E. Shanks, Removal of heavy metals and other cations from wastewater using zeolites, Sep. Sci. Technol. 25 (1990) 1555–1569.
[34] R. Han, Z. Lu, W. Zou, W. Daotong, J. Shi, Y. Jiujun, Removal of copper(II) and lead(II) from aqueous solution by manganese oxide coated sand, J. Hazard. Mater. 137(1) (2006) 480–488.
[35] P.C. Mishra, R.K. Patel, Removal of lead and zinc ions from water by low cost adsorbents, J. Hazard. Mater. 168(1) (2009) 319–325.
[36] M.I. Martín, F.A. López, C. Pérez, A. López-Delgado, F.J. Alguacil, Adsorption of heavy metals from aqueous solutions with by-products of the steelmaking industry, J. Chem. Technol. Biotechnol. 80(11) (2005) 1223–1229.
[37] M.A.O. Badmus, T.O.K. Audu, B.U. Anyata, Removal of lead ion from industrial wastewaters by activated carbon prepared from periwinkle shells (*Typanotonus fuscatus*), Turkish J. Eng. Environ. Sci. 31(4) (2007) 251–263.
[38] V.K. Gupta, I. Ali, Removal of lead and chromium from wastewater using bagasse fly ash—A sugar industry waste, J. Colloid Interface Sci. 271(2) (2004) 321–328.
[39] S.K. Srivastava, R. Tyagi, N. Pant, Adsorption of heavy metal ions on carbonaceous material developed from the waste slurry generated in local fertilizer plants, Water Res. 23 (1989) 1161–1165.
[40] K. Biswas, S.K. Saha, U.C. Ghosh, Adsorption of fluoride from aqueous solution by a synthetic iron (III)−aluminum(III) mixed oxide, Ind. Eng. Chem. Res. 46 (2007) 5346–5356.
[41] E.I. Unuabonah, K.O. Adebowale, B.I. Olu-Owolabi, Kinetic and thermodynamic studies of the adsorption of lead(II) ions onto phosphate-modified kaolinite clay, J. Hazard. Mater. 144 (2007) 386–395.